Digest Journal of Nanomaterials and Biostructures Vol. 20, No. 4, October-December 2025, p. 1425-1436

Environmentally friendly PVP /ZnO/Ag nanocomposite based organic solar cells

B. Karunamoorthy [a], A. Ahila [b], S. Vimala Rani [c,*], Sampath Pondurai [d]
[a] *Associate Professor, Dept of Electrical and Electronics Engineering, Kumaraguru College of Technology, Coimbatore, India*
[b] *Associate Professor, Dept of ECE, Sri Sairam College of Engineering, Bangalore, India*
[c] *Corresponding author, Vel Tech Rangarajan Dr. Sagunthala R&D Institute of Science and Technology, Chennai, India*
[d] *Research scholar, NIT Calicut, India*

This study investigates the development of effective polyvinyl pyrrolidone (PVP)-based organic solar cells (OSCs) incorporating zinc oxide nanoparticles (ZnO NPs) as the electron transport layer and silver nanoparticles (Ag NPs) as the acceptor. The primary objective was to optimize charge extraction and reduce resistance through precise control over the deposition of PVP/ZnO/Ag nanocomposite as active layers. Comprehensive characterization using UV-Vis, FTIR, SEM, EDX, and XRD confirmed the successful synthesis of crystalline ZnO and FCC Ag nanoparticles and revealed a beneficial highly branched, coral-like morphology for the composite films. Device performance was analytically assessed for varying coating thicknesses of active layer. The OSC with an optimized thickness is achieved with two coatings (250-280 nm) demonstrated superior photovoltaic performance under 100 mW/cm² broadband illumination, with a PCE of 2.11%, short-circuit current (JSC) of 12.5 mA, an open-circuit voltage (VOC) of 188 mV, and a fill factor (FF) of 78%. The inclusion of Ag NPs was crucial for enhancing electron extraction, while the uniform, branched morphology facilitated efficient charge transport. This work highlights the significant potential of PVP/ZnO/Ag nanocomposites for developing high-performance, cost-effective organic solar cells for practical applications.

(Received July 22, 2025; Accepted November 11, 2025)

Keywords: OSC, Ag NPs, OPVs, BHJ, PCE, fill factor, Short circuit current

1. Introduction

Organic solar cells have received important consideration due to their prospective low-cost energy conversion [1]. The bulk heterojunction (BHJ) structure of organic donor and acceptor materials makes up the active layer of these cells, together with charge transporters and transparent conductive electrodes [2]. The optical and electrical characteristics of OSCs can be adjusted using nanosol-based methods, which are also reasonably priced to produce [3]. As emphasized by Clarke and Durrant (2010) [4], rigorous investigation and production of effective donor and acceptor materials are necessary to improve OSC efficiency. However, they have drawbacks like as lower efficiency, instability, and sensitivity to outside influences in comparison to silicon solar cells. In order to enhance OSC performance more research into new materials is needed [5]. Scientists are exploring the combination of nanoparticles such as zinc oxide (ZnO) and silver nanoparticles (AgNPs) to boost the performance of batteries and organic solar cells (OSCs) [6]. ZnO is favored in solar cells due to its excellent optoelectronic properties, affordability, and ease of production, non-toxicity, and high stability [7]. It is used as a transparent electrode or buffer layer and acts as an electron acceptor in ZnO/organic heterojunction solar cells (HSCs) [8]. Enhancing the structure of ZnO is a key to improving the performance of these devices. Incorporating AgNPs into ZnO in bulk heterojunction (BHJ) devices enhances the stability of OSCs, as well as excitation separation and charge transfer [9]. While ZnO has a lower absorption coefficient compared to materials like

* Corresponding author: ashavimala@gmail.com
https://doi.org/10.15251/DJNB.2025.204.1425

silicon or perovskites, its use in specific configurations, as electron transport layers in inverted organic photovoltaic cells, can still significantly enhance solar cell performance [10].

The impact of these materials on important characteristics like charge mobilities, molecular energy levels, and absorption spectra are investigated to better understand how they affect device performance [11, 12]. According to Xie et al. (2011) [11], Ag NPs can improve charge extraction in OSCs by decreasing the work function of the electron transport layer, hence increasing electron transfer in organic solar cells [13]. The internal charge rearrangement of the NPs-TiO2 metal system helps with charge extraction, resulting in higher photocurrent and power conversion efficiency [14]. As ZnO/AgNPs has superior optical and electrical conductivity than pure ZnO, polymer solar cells (PSCs) may effectively use them [15]. Through light-trapping, AgNPs optimize light absorption and minimize energy losses, increasing the short-circuit current density (Jsc) and ultimately increases the efficiency of solar cells (ɳ) [16, 17].

In the presence of solar light, the accumulation of charges in composite materials significantly enhances charge extraction [6, 18]. This work focused on the incorporation of PVP-ZnO/Ag Nanocomposites into OSC structures to enhance device performance and impact power conversion efficiency. Application inferences of the results are also discussed, to develop improved OSCs suitable for everyday applications (refer scheme 1). Although the study focuses primarily on optimising device thickness, it also highlights the potential and usefulness of OSCs for a wide range of applications [19]. By addressing issues with energy sustainability and climate change, this study highlights how proposed OSC could help in the development of sustainable energy solutions.

2. Experimental method

A simple layer by layer solution-deposition method has been developed for manufacturing polymer solar cells (PSCs) with a PVP/ZnO/Ag bilayer cathode, which is improved by incorporating a self-assembly monolayer (SAM) modification. Heat is applied to speed up the deposition process. This modification enhances the interface between the active layer and cathode, leading to higher power conversion efficiency. The technique is low-cost, straightforward, and ideal for large-scale production. Additionally, using silver nanoparticles (AgNPs) as effective antennas on ZnO nanoparticles significantly improves light harvesting and minimizes energy losses, further boosting PSC performance. This innovative approach provides an economical and scalable solution for producing organic optoelectronic devices.

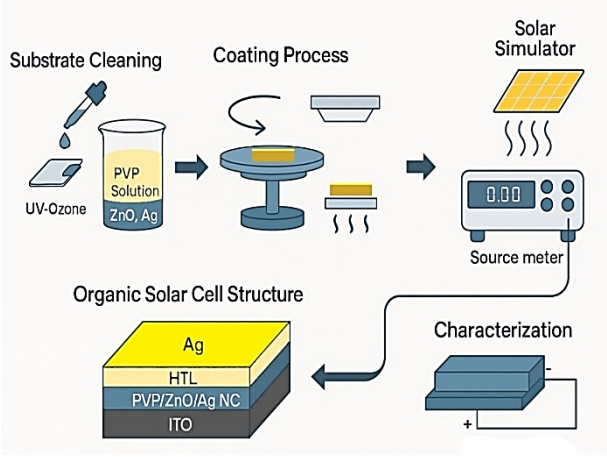

Scheme 1. Graphical representation of proposed OSC.

2.1. Instrumentation

UV-vis absorption spectroscopy was carried out using a Marutek MAR-2020 fiber optic spectrometer. The surface variation and classification ZnO and AgNPs were determined using an Agilent Technologies Cary 630 FTIR System (Varian, USA). The surface morphology was identified using a scanning electron microscope (SEM) from Tescan Vega in the Czech Republic, and the particle size distribution was calculated using ImageJ software. Image interpretation is carried by using software tools such as ImageJ and OriginPro 2024.

To measure current-voltage (I-V) characteristic curves during electrical testing, a DC power supply type DF1730SB3A was utilized. Furthermore, room temperature and natural light levels were used for these measurements. With 20 mV increments, the voltage was raised from a starting value of 0V to about 1V. By taking into account elements like conductivity and the behavior of charge carriers in the material, this technique made it possible to evaluate the electrical properties of the films.

3. Preparation of chemical

3.1. Sol-Gel technique for producing ZnO nanoparticles

ZnO nanoparticles were made exactly as described in the paper by Immanuel et al. (2023)[8]. In brief, 0.2 grams of CTAB were mixed in 100 milliliters of deionized water, then 1 milliliter of a 2% zinc acetate solution was added, and the mixture was stirred at 500 revolutions per minute. NaOH was added gradually in droplets until the solution became cloudy. After letting the mixture sit for 30 minutes, it was cooled, centrifuged, and the solid that formed was washed with water and ethanol. In the end, the solid was subjected to a temperature of 350 °C for duration of 2 hours in order to produce ZnO nanoparticles [9]. After undergoing calcination, the solution displays a prominent 340 nM peak under the UV-Visible spectrometer, which is considered a significant peak for ZnO NPs (see figure.1).

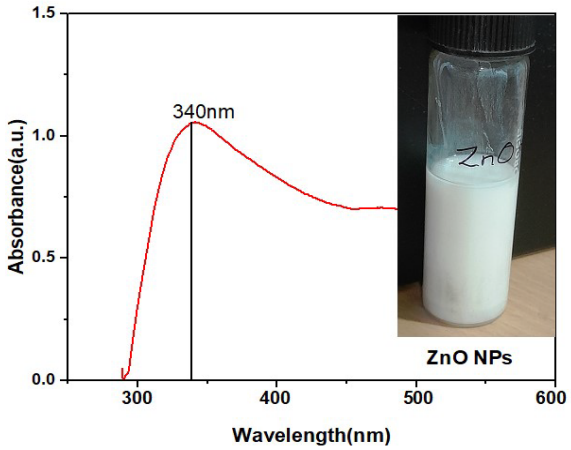

Fig. 1. UV-Vis absorption spectrum of ZnO NPs with inset showing the nanosol.

3.2. Preparation of AgNPs

Silver nanoparticles (Ag NPs) were produced using the procedure detailed by Samuel and Rao (2024)[10], with minor adjustments. 10 mL of 2.0×10^{-3} M $AgNO_3$ solution was added to a 50 mL Erlenmeyer flask, and the pH was set to 5 with 25 µL of PAH. By stirring at 650 rpm, a solution of Ag NPs in a light-yellow color was formed after adding 1 mM $NaBH_4$ as a reducing agent. Following that, 100 µL of 1 mM CTAB was introduced, resulting in the solution transitioning to a deep dark brown color, signifying the creation of PAH-capped Ag NPs (PAH-Ag

NPs) showing absorption spectrum at 425 nM under UV-Visible absorption spectrometer. These PAH-Ag NPs remained unchanged at room temperature for more than a month (refer figure.2).

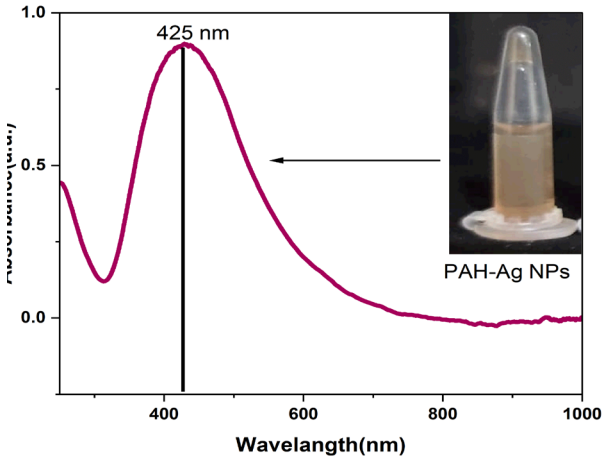

Fig. 2. UV-Vis absorption spectrum of Ag NPs with inset showing the nanoparticle sol

4. Results and discussion

4.1. Characterization of Ag and ZnO NPs

4.1.1. SEM of PAH-Ag NPs

After synthesizing the AgNPs in ultra-pure water, a drop of the solution was applied to a clean silicon chip, and it was allowed to air dry for scanning electron microscopy investigation. Strong cationic polymer PAH is used to functionalize the nanoparticles, producing positively charged[19], uniformly distributed silver nanoparticles(Fig.3a) that range in size from 40 to 55 nm. The particle size distribution graph (Fig.3b) indicated that the generation of silver nanoparticles was spherical and generally uniform in size, with diameters ranging from 40 to 55 nm, as seen in the SEM image.

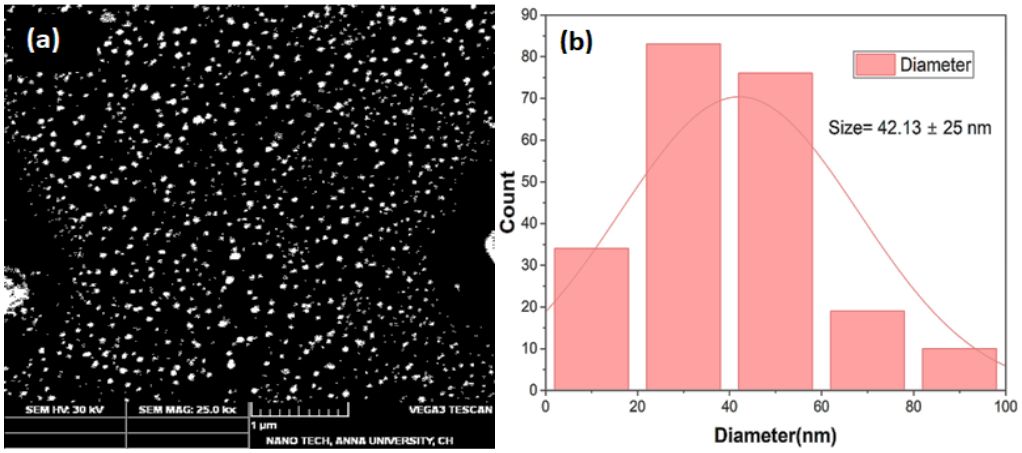

Fig. 3. (a) SEM image of PAH-Ag NPs and (b) its Particle size distribution graph.

4.1.2 SEM of ZnO NPs

Scanning electron microscopy is used to evaluate the quality of zinc oxide nanofractals (NFs) and intergenerational, stacked ZnO NPs. Nanofractals with long, branching patterns and

multigenerational branches (ref Fig.4a and 4b) improve power conversion efficiency[20]. This is due to increased dye loading, light harvesting, and a reduced charger combination. Heat treatment improves the performance of stacked ZnO NP to transfer electrons from photo anodes. The approach imitates branching plant structures in order to absorb more solar light.

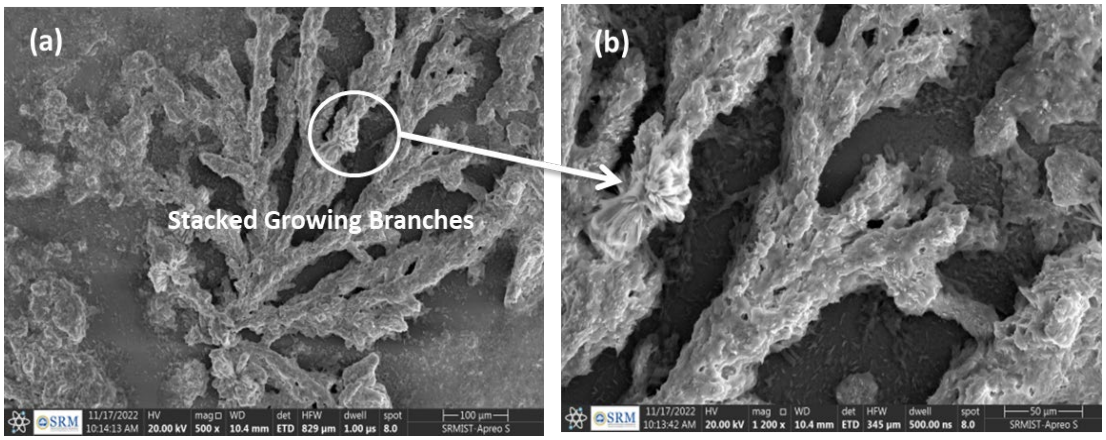

Fig. 4. (a and b) Low and High dimension SEM images of ZnO Nano fractals and its stacked branches.

4.2. EDX

The elemental analysis technique known as energy dispersive x-ray (EDX) microanalysis is related to electron microscopy and is based on the generation of characteristic x-rays that reveal the presence of elements in the material. EDX analysis verified the presence of elemental Ag and Zn in the sample, pointing to the synthesis of ZnO and AgNPs. The graph (figures 5a and 5b) shows the highest values of absorption of Ag at 3.6 keV and Zn at 8.4 keV. Other Functional materials introduced throughout the synthesis process cause elemental peaks to appear. The production of AgNPs was confirmed by the presence of elemental Ag in the sample by EDX analysis. The graph (Fig.5a) shows the Ag absorption peak at 3.7 keV. The other peaks' N, H, and S concentrations suggest the presence of PAH.

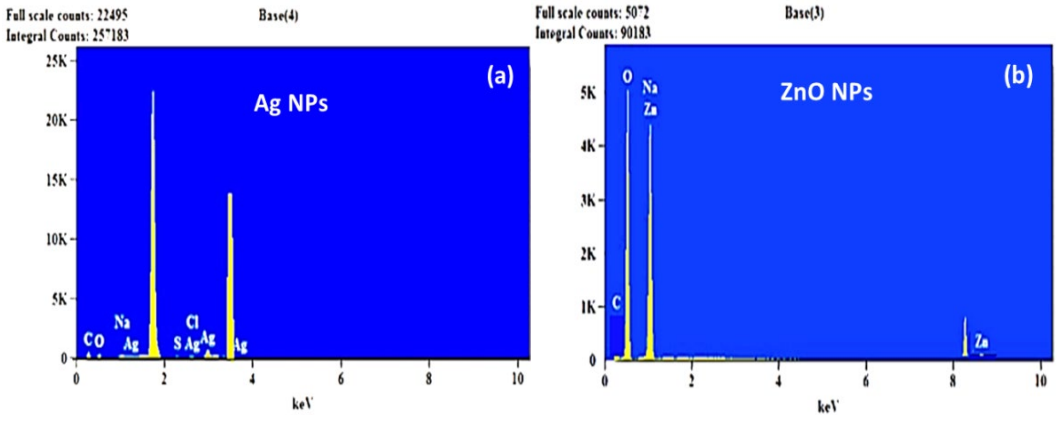

Fig. 5. EDX analysis graph of PAH-Ag NPs(a) and ZnO NPs(b).

4.3. XRD

The XRD studies indicate that the PAH–AgNPs generated were within the nano crystal range (ref Fig .6a), as indicated by the peaks at 2θ values of 38°, 44.3°, 64.5°, and 77.35° associated with the (111), (200), (220), and (311) planes, which are silver's Braxton–Bragg

reflections (Lee and Jun 2019). A few minor intensity peaks were also present, denoted by the sign *. These may result from certain precursors serving as stabilizing agents while the process is underway. Using XRD measurements and the Debye-Scherer equation, the average diameter of the silver nanoparticles was determined to be 40.38 ± 3.5 nm. The AgNPs created were clearly Nano crystalline, proven by structural peaks in XRD patterns and an average crystal size of around 40 nm by Debye Scherer equation.

$$D = \frac{k\lambda}{(\beta * \cos\theta)} \quad [21]$$

The X-ray diffraction pattern of a ZnO sample calcined at 350ºC is given in Fig.6b. According to standard data JCPDS 76-0704, the synthesized material has a ZnO phase (wurtzite structure). The peak measured for ZnO are reliable with literature values [9]. There were no impurity characteristic peaks found. The peaks observed at scattering angles of 31.94°, 34.95°, 36.65°, 46.9°, 57.82°, 63.45°, and 69.2° correspond to crystal planes with Miller indices (100), (002), (101), (102), (110), (103), and (112). The X-ray diffraction pattern of ZnO nanoparticles indicates an average crystal size of 41 nm, as determined by applying the Williamson Hall analysis [23].

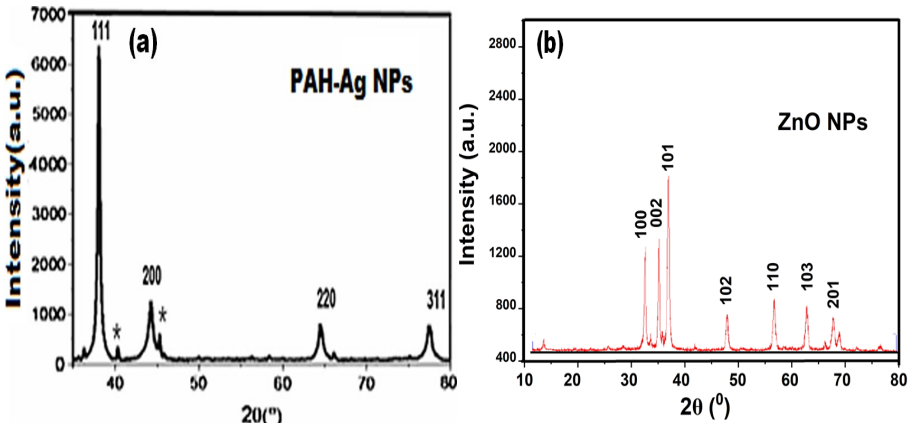

Fig. 6. (a) XRD Analysis of PAH-Ag NPs and (b) ZnO NPs.

4.4. FTIR

4.4.1. PAH-Ag NPs

As reported by Lin et al. (2010), the substance exhibited N-H stretching within the range of 3400 to 3600 cm−1.The asymmetric N-H stretching pulse of the NH^{3+} group caused by the amine group in PAH was the cause of the elongation at 1643.8 cm−1[22]. Ashrafi et al. (2018) state that the peak in PAH at 1454.3 cm−1 represents the principal amine's N-H bending vibration, which is utilized to functionalize AgNPs [23]. The CH2-NH3 bond is indicated by the peak at 1017 cm−1. The functionalization of AgNPs with PAH was validated by the FTIR study (Fig.7).

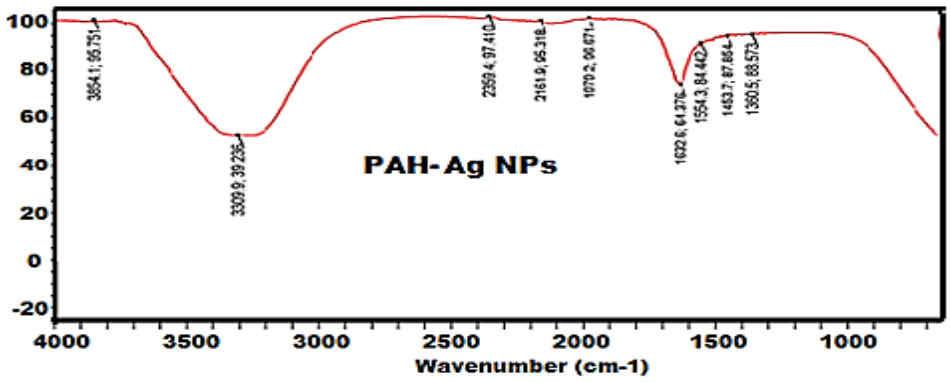

Fig. 7. FT-IR analysis of PAH-Ag NPs.

4.4.2. ZnO NPs

FT-IR analysis was conducted on the zinc nanoparticles that were synthesized to detect the different functional groups linked to them. The absorption peaks that result show the specific functional groups that are found in the zinc oxide nanoparticles. The peak observed at 575.9 cm-1 is related to the stretching vibrations of ZnO, showing the presence of metal-oxygen bonds [6]. The 1005.3 cm-1 peak is associated with the stretching vibration of either the C-N bond in primary amines or the C-O bond in primary alcohols. The peaks observed between 1100cm-1 and 1384cm-1 correspond to the in-plane bending or vibration of primary and secondary alcohols. The vibration modes of aromatic nitro compounds and alkyl groups are represented by the peak at 1572.7 cm-1. At last, the peaks observed at 2929.8 cm-1 and 3295.8 cm-1 are assigned to the stretching vibration of hydroxyl groups[7].

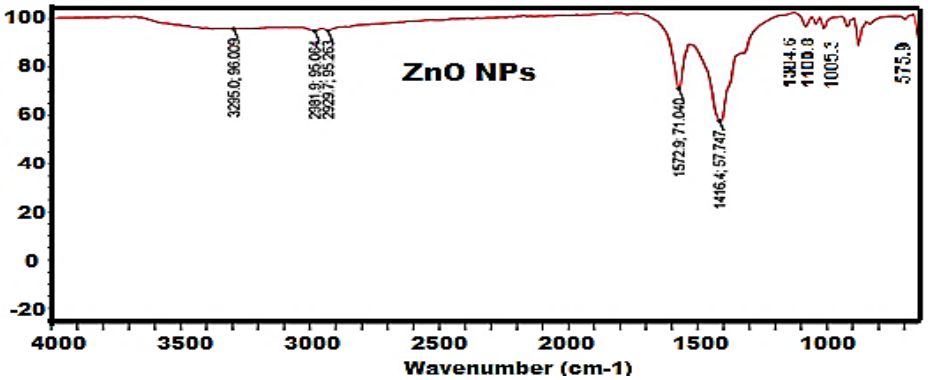

Fig. 8. FT-IR analysis of ZnO NPs.

5. Preparation of thin-film organic solar cell

The PVP/ZnO/Ag nanocomposite-based organic solar cell was created by synthesizing nanocomposite materials and then methodically fabricating the device. First, a solid-state technique adapted from Rabee et al., 2022 was used to create ZnO and Ag nanoparticles [24]. After being finely ground, the nanoparticles were dried for four hours at 60°C. A 1% (w/v) solution of polyvinylpyrrolidone (PVP), which served as a stabilizing polymer matrix, was then used to disperse these. The nanocomposite solution was exposed to ultrasonic treatment for 15 minutes in order to ensure uniform dispersion and avoid agglomeration. The resultant solution was drop-cast for bulk film studies and left to dry for 24 hours at room temperature (or heated slightly to speed up drying). Indium tin oxide (ITO)-coated glass substrates were cut into 2.5 cm × 2.5 cm pieces and ultrasonically cleaned in acetone, isopropanol, and deionized water in order to fabricate

the device. After being dried with nitrogen, the substrates were exposed to UV-ozone for 15 to 20 minutes in order to increase surface energy. After filtering PEDOT:PSS, it was spin-coated onto the treated substrates for 40 seconds at 3000 rpm and then baked for 10 minutes at 120 °C to create a hole transport layer (HTL). The active layer was then created by spin-coating the PVP/ZnO/Ag nanocomposite solution over the PEDOT:PSS layer. To guarantee film homogeneity, single, double, and triple coatings were made, and each layer was baked for 10 to 15 minutes at 80 to 100 °C. A digital Vernier caliper was used to measure film thickness in order to correlate it with device performance. After that, 100 nm of silver (Ag) was thermally evaporated through a shadow mask at high vacuum to deposit the cathode. Before being removed, the devices were cooled, and encapsulation was an option to stop deterioration. In order to optimize the active layer thickness for increased photovoltaic efficiency, electrical characterization was carried out using a source meter under AM1.5G solar illumination (100 mW/cm²). Device performance with varying coating numbers (thickness) were compared.

6. Device performance evaluation

Each component of the organic solar cell contributes significantly to the device's efficiency. The OSC layer, which is typically 120 and 620 nm thick, is critical to the photovoltaic device's performance because it effects light absorption efficiency, exciton dissociation, and charge carrier transportation(25).ZnO nanoparticles act as an ETL, encouraging electron flow while also blocking holes to reduce recombination. Furthermore, ZnO's high-energy conduction band enables effective electron collection [15].

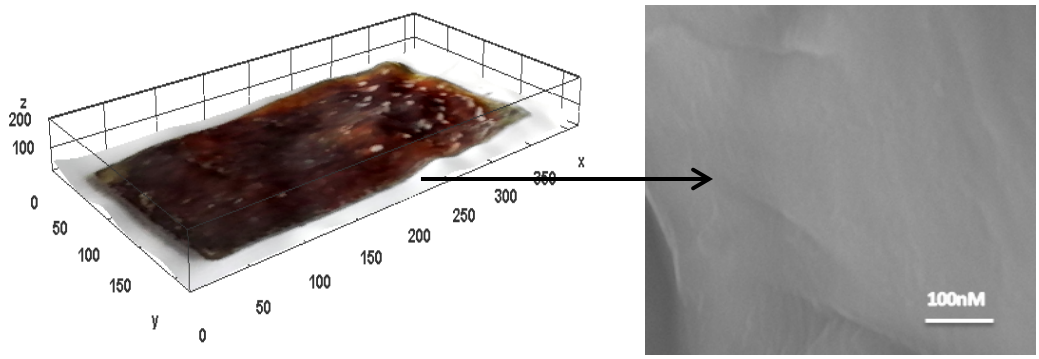

Fig. 9. Representative Surface Plot and SEM image of thin film OSC deposited on a SiO glass substrate exhibiting a smooth surface.

The top electrode is composed of silver nanoparticles (Ag NPs), which form a conductive channel for electron extraction. Their equal distribution contributes to a strong electrical connection with the active layer, reducing series resistance and improving charge extraction[16] .Silver (Ag) is considered the most suited and reliable electrode among all high-performance metals. An oxidation procedure can increase the work function by nearly 0.7 eV, making it better suited for hole extraction [17].

The surface plot profile and SEM picture (Figure 9) reveal that the films have a smooth surface (figure.9), which is consistent with the OSC performance described in Table 1 [18].These materials interact to improve charge transport, reduce recombination losses, and improve charge collecting, resulting in a significant boost in total OSC efficiency [19]. UV-vis spectroscopy and I-V studies offered a full understanding of the films' optical and electrical properties, which was critical for establishing their potential for application in organic solar cells. Table 1 summarizes the total device performance. UV-vis spectroscopy was used to evaluate the films' light absorption

capacities, which is critical for photovoltaic efficiency. I-V curve offered information on the charge transport features (figure 10).

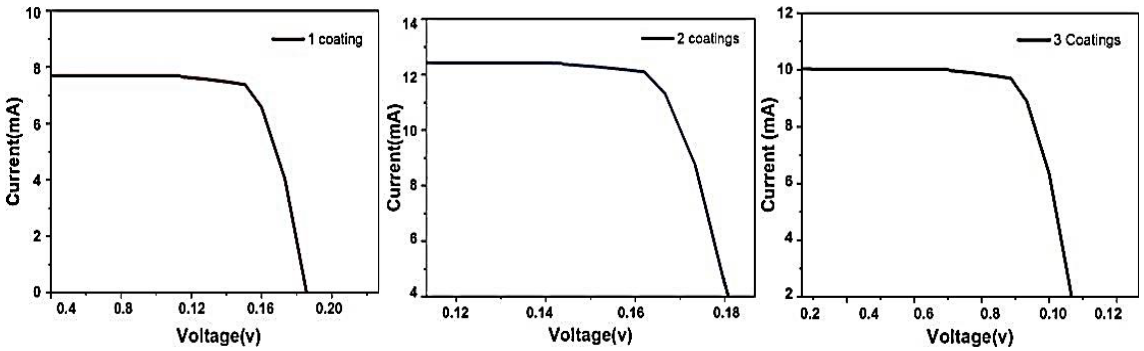

Fig. 10. I-V curve of the proposed OSC with different coatings (1, 2, 3).

Table 1. Performance summary of the proposed OSC

Coatings	Film thickness (nm)	L (mW/cm^2)	Current (mA)	P_{max} (mW)	VOC (mV)	(FF) (%)	PCE (%)	
1	125-142	100	7.8	1.125	186.4	76.7	1.29%	
2	250-280	100	12.5	1.845	188	78.5	2.11%	
3	500-620	100	10	0.784	108	72.6	0.90%	

When exposed to broad light with a power of 100±2 mW/cm^2, the OSC shows a maximum short circuit current I_{SC} of 12.5 mA, an Open circuit voltage V_{OC} of 188 mV, and a FF of 78.5% (figure 10). These factors result in a power conversion efficiency of 2.11 %, determined by the equation:

$$\eta = FF * Isc * Voc/IL \quad [22]$$

where

$$FF = VMPP.IMPP \,/\, P\,Light \quad [27]$$

6.1. Comparison of solar cell performance

Among the fabricated devices, the solar cell with two coatings of the PVP/ZnO/Ag nanocomposite exhibited the highest power conversion efficiency (PCE) of 2.11%, outperforming the single-coating (1.29%) and triple-coating (0.90%) devices.

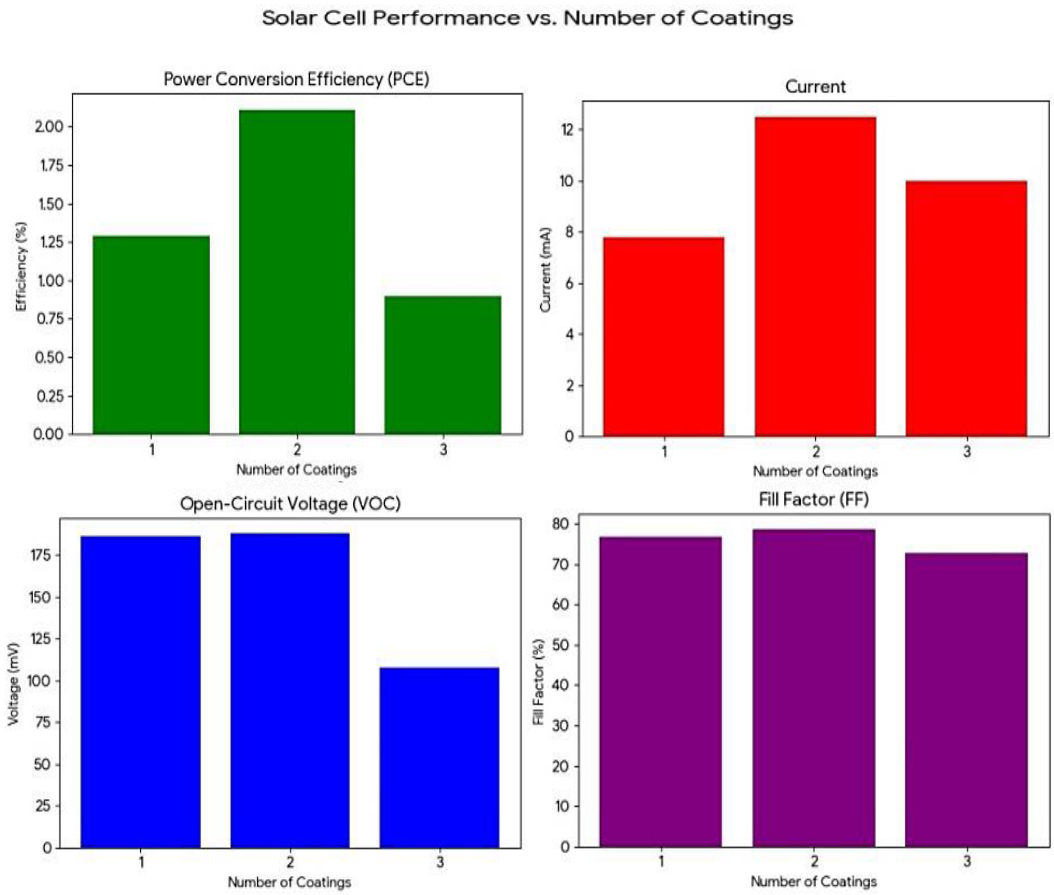

Fig. 11. Comparative chart of overall device performance based on the coatings.

This enhancement in efficiency is attributed to a balance between adequate light absorption and effective charge transport. The two-coating device also demonstrated the highest short-circuit current (12.5 mA) and maximum output power (1.845 mW), indicating superior photogenerated charge generation and extraction. Furthermore, it exhibited the highest fill factor (FF) of 78.5%, signifying improved film quality and optimal thickness for efficient charge carrier collection. In contrast, the single-coating device, while relatively efficient, likely suffered from limited light absorption due to its thinner active layer. On the other hand, the triple-coating device, despite higher material content, showed a significant drop in performance, possibly due to excessive film thickness (500–620 nm) leading to increased charge recombination and series resistance (refer figure 11).

7. Conclusion

In summary we have demonstrated the efficiency of OSC coated with PVP/ZnO/Ag nanocomposites as active layer with 3 different coating thicknesses. This study successfully developed and optimized PVP-based organic solar cells (OSCs) integrating ZnO and Ag nanoparticles. Comprehensive characterization confirmed the formation of crystalline nanoparticles and a beneficial branched, coral-like film morphology. Optimal device performance with PCE of 2.11%, VOC 188 mV, JSC 12.5 mA, FF 78% was observed in active layer with two coatings (250-280 nm thickness). The Ag NPs enhanced electron extraction, and the unique morphology facilitated efficient charge transport.

These findings suggest that the two-coating configuration yields an active layer of optimal thickness and morphology, achieving a favorable balance between photon absorption and charge extraction, thereby maximizing overall device performance. This work underscores the significant potential of this nanocomposite system for practical photovoltaic applications, while highlighting the importance of precise morphological control.

References

[1] Peumans P, Yakimov A, Forrest SR., J Appl Phys. 2003;93(7):3693-723; https://doi.org/10.1063/1.1534621

[2] Weng K, Ye L, Zhu L, Xu J, Zhou J, Feng X, et al., Nat Commun. 2020 Jun 5;11(1):2855; https://doi.org/10.1038/s41467-020-16621-x

[3] Han G, Zhang S, Boix PP, Wong LH, Sun L, Lien SY., Prog Mater Sci. 2017;87:246-91; https://doi.org/10.1016/j.pmatsci.2017.02.003

[4] Clarke TM, Durrant JR., Chem Rev. 2010 Nov 10;110(11):6736-67; https://doi.org/10.1021/cr900271s

[5] Hoppe H, Sariciftci NS., J Mater Res. 2004;19(7):1924-45; https://doi.org/10.1557/JMR.2004.0252

[6] Immanuel AJ, Samuel VR, Devi MY, Rajee SAM., Phys Scr. 2023;98(10):105909; https://doi.org/10.1088/1402-4896/acf3b0

[7] Ko SH, Lee D, Kang HW, Nam KH, Yeo JY, Hong SJ, et al., Nano Lett. 2011 Feb 9;11(2):666-71; https://doi.org/10.1021/nl1037962

[8] Oseni SO, Mola GT., Sol Energy Mater Sol Cells. 2017;160:241-56; https://doi.org/10.1016/j.solmat.2016.10.036

[9] Faisal S, Jan H, Shah SA, Shah S, Khan A, Akbar MT, et al., ACS Omega. 2021 Apr 13;6(14):9709-22; https://doi.org/10.1021/acsomega.1c00310

[10] Alhuyi Nazari M, Maleki A, Assad MEH, Rosen MA, Haghighi A, Sharabaty H, et al., Sol Energy. 2021 Nov 1;228:725-43; https://doi.org/10.1016/j.solener.2021.08.051

[11] Tsimpliaraki A, Tsivintzelis I, Marras SI, Zuburtikudis I, Panayiotou C., J Supercrit Fluids. 2011 Jul 1;57(3):278-87; https://doi.org/10.1016/j.supflu.2011.03.010

[12] Toh HS, Batchelor-McAuley C, Tschulik K, Compton RG., Sci China Chem. 2014;57(9):1199-210; https://doi.org/10.1007/s11426-014-5141-8

[13] Zhao W, Li S, Yao H, Zhang S, Zhang Y, Yang B, et al. ACS Publications. American Chemical Society; https://doi.org/10.1021/jacs.7b02677

[14] Zhang X, Du Z, Zhu Y, Li C, Hu X, Yang T, et al., Sol Energy Mater Sol Cells. 2020;207:110366; https://doi.org/10.1016/j.solmat.2019.110366

[15] Otieno F, Mutuma BK, Airo M, Ranganathan K, Erasmus R, Coville N, et al., Thin Solid Films. 2017 Mar 1;625:62-9; https://doi.org/10.1016/j.tsf.2017.01.047

[16] Xie F., Curr Food Sci Technol Rep. 2023 Sep 1;1(1):1-12; https://doi.org/10.1007/s43555-023-00002-8

[17] Chang Y, Zhu X, Lu K, Wei Z., J Mater Chem A. 2021;9(6):3125-50; https://doi.org/10.1039/D0TA10594E

[18] Samuel VR, Rao KJ., Appl Nanosci. 2024 Jan;14(1):33-42; https://doi.org/10.1007/s13204-023-02948-6

[19] Samuel VR, Rao KJ., Results Opt. 2023;13:100513; https://doi.org/10.1016/j.rio.2023.100513

[20] Wibowo A, Agung Marsudi M, Ikhlasul Amal M, Bagas Ananda M, Stephanie R, Ardy H, et al., RSC Adv. 2020;10(70):42838-59; https://doi.org/10.1039/D0RA07689A

[21] Samuel VR, Rao KJ., Chem Phys Impact. 2023 Jun;6:100161; https://doi.org/10.1016/j.chphi.2023.100161

[22] Lee SH, Jun BH., Int J Mol Sci. 2019 Jan;20(4):865; https://doi.org/10.3390/ijms20040865

[23] Ashrafi AM, Koudelkova Z, Sedlackova E, Richtera L, Adam V., J Electrochem Soc. 2018 Dec 11;165(16):B824; https://doi.org/10.1149/2.0381816jes

[24] Rabee B, Mundher S, Shakir F., Synthesis of (PVA-PVP: ZnO and Ag) Nanocomposite Films: Characterization and Antibacterial Application, 2022 Jul 2;20:738-46.

[25] Xu T, Chen Q, Huang G, Zhang Z, Gao X, Lu S., Sol Energy Mater Sol Cells. 2016;155:141-6; https://doi.org/10.1016/j.solmat.2016.06.003

[26] Fukuda K, Yu K, Someya T., Adv Energy Mater. 2020 Jul;10(25):2000765; https://doi.org/10.1002/aenm.202000765

[27] Kietzke T., Adv Optoelectron., 2007; https://doi.org/10.1155/2007/40285